Micromagnetic Modelling of Nanocomposite Magnets

Thomas Schrefl, Josef Fidler and Dieter Süss

Institute of Applied and Technical Physics, Vienna University of Technology,
Wiedner Hauptstraße 8-10, A-1040 Vienna, Austria

Abstract

Finite element modelling treats magnetization processes within on a length scale of several nanometers and thus give a quantitative correlation between the microstructure and the magnetic properties of nanocomposite magnets. The numerical solution of the Gilbert equation of motion shows how reversed domains nucleate and expand. Magnetization reversal starts at the grain boundaries disolving a strongly nonuniform magnetic state. The intrinsic magnetic properties near the grain boundaries strongly influence the remanence and the coercive field of two phase, nanocrystalline magnets. The magnetic properties are assumed to gradually decrease from their bulk values in the intergranular phase. A linear reduction of the exchange constant to 20% of its bulk increases the coercive field by up to 50% percent without a significant reduction of the remanence in NdFeB/α-Fe magnets with a mean grain size of 10 nm.

1. Introduction

Nanocomposite permanent magnets have been widely studied experimentally and theoretically during the last decade [1-12]. These magnets consist of a mixture of magnetically hard and soft phases. Nanocomposite magnets show a high remanence and a reasonable large coercive field, if both phases are sufficiently exchange coupled. Nanocomposite magnets with excellent hard magnetic properties were obtained for various different compositions. The soft magnetic phase is either α-Fe or Fe_3B. As hard magnetic phase $Nd_2Fe_{14}B$, $SmCo_5$, $Sm_2Fe_{14}N_x$, and $Pr_2Fe_{14}B$ were used. Possible application of nanocomposite permanent magnets are bonded magnets used in consumer electronic applications, where the miniaturization requires magnets that are easy to magnetize [12-13]. In addition, the reduction of the total rare-earth content may lead to a cost reduction. Whereas the enhanced remanence of nanocomposite magnets is an advantage as compared to isotropic, single-phase nanocrystalline NdFeB magnets, the coercive field obtained in two-phase systems is rather low. Thus recent studies investigated different ways to improve the coercive field of nanocomposite magnets. Hirosawa and co-workers showed that the hard magnetic properties of nanocomposite magnets can be significantly improved by modifying the alloy compositions [9]. The substitution of Nd by Dy [9] or [10] increases the hard phase anisotropy, giving rise to an improved coercivity without a significant loss in remanence. Fukunga and co-workers [6] proposed a two-phase microstructure consisting of NdFeB and α-Fe grains embedded within a residual amourphous phase, in order to improve the coercive field of nanocomposite magnets. Such a nanocomposite system was realized by Hamano and co-workers [11] using a composition $Nd_8Fe_{76}Co_8Nb_2B_6$ with a maximum H_c = 575 kA/m.

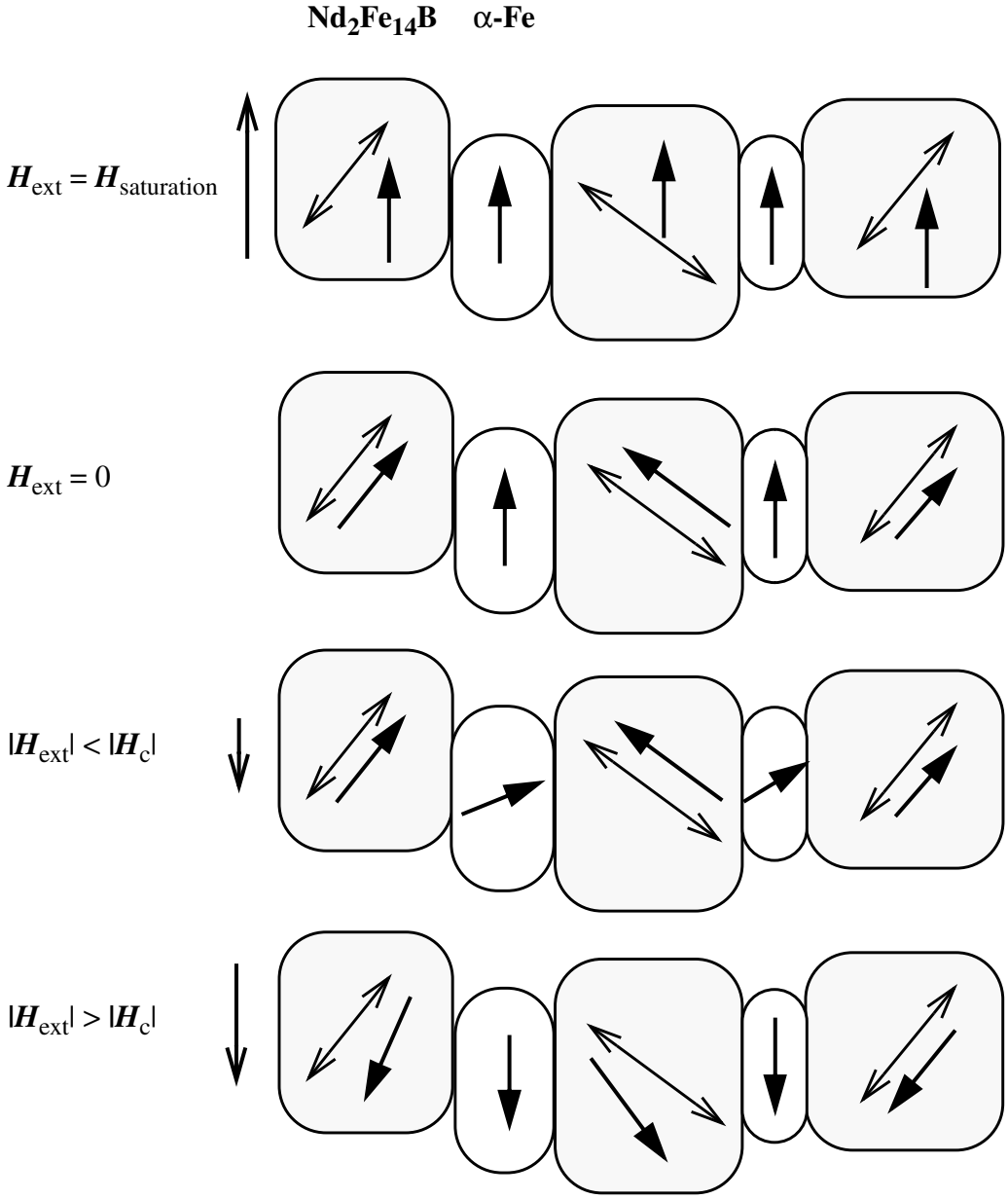

Figure 1: Schematics of remanence enhancement and magnetization reversal in two-phase nanocrystalline permanent magnets. The magnetocrystalline anisotropy directions of the hard phase (dark) are randomly oriented. At zero applied field, the magnetization of the soft phase (bright) points parallel to the average magnetization direction of neighboring hard magnetic grains. At the critical field exchange interactions between the hard and the soft phase causes the irreversible switching of a neighboring hard magnetic grain.

Figure 1 schematically illustrates remanence enhancement and magnetization reversal in two-phase nanocrystalline permanent magnets. In order to explain the influence of intergrain exchange interactions, Kneller [1] proposed a model where the magnetization of the different phases are connected by mechanical springs. At a high external field, the magnetization of all grains

becomes oriented upwards. As the field is gradually reduced to zero the magnetization of the hard magnetic grains rotate towards the direction of their local easy axes. The magnetization of the soft magnetic grains remains parallel to the saturation direction. The springs of neighboring hard magnetic grains like to pull the magnetization into different directions. These competitive effects cancel and at zero applied field, the magnetization of the soft phase points parallel to the average magnetization direction of neighboring hard magnetic grains. Under the influence of a reversed external field, the magnetization of the soft phase rotates reversibly. If the field is removed, the magnetization of the soft grains will rotate back to its original direction which is the so called exchange-spring effect. At higher opposing fields the magnetization of the soft grains may even point downwards. The connecting springs provide a high torque onto the neighboring hard magnetic magnetization, leading to the irreversible switching of the hard magnetic grains. A reduction of the stiffness constant reduces the torque onto the hard magnetization and thus shifts irreversible switching towards higher values of the opposing field. An apropriate choice of the exchange stiffness will keep remanence enhance and improve the coercive field. Thus it is possible to tailor the magnetic properties of nanocomposite magnets changing the amount and the intrinsic properties of an intergranular phase. An apropriate reduction of the intergrain exchange may improve the coercive field but still keep the effect of remanence enhancement.

Inoue [2] and Hamano [3] successfully prepared α-Fe/$Nd_2Fe_{14}B$ magnets with a remaining amorphous phase. The amorphous intergranular phase is expected to reduce the exchange interactions between the hard and the soft grains, leading to an improved coercive field. A coercive field of H_c = 405 kA/m was obtained for nanocomposite magnets produced from a $Nd_8Fe_{76}Co_8Nb_2B_6$ melt-spun alloy. The corresponding remanence and energy density product were $J_r = 1.16$ T and $(BH)_{max} = 147$ kJ/m^3 [3]. Atom probe characterization of $Nd_8Fe_{76.5}Co_8B_6Nb_1Cu_{0.5}$ show that intergranular phase is enriched with Nb and B [4]. Mössbauer studies by Kobayshi and co-workers [5] suggest that the proposed intergranular phase is actually ferromagnetic with magnetic properties that gradually decrease towards the grain boundary.

Recently, Fukunaga and co-workers [6] numerically investigated the effect of reduced strength of intergrain exchange interactions in α-Fe/$Nd_2Fe_{14}B$ systems. Their results confirm the increase of coercivity owing to reduced intergrain exchange interactions, provided that grain size is sufficently small. The increase of coercive field without a significant loss of the remanence enhances the energy density product. A reduction of the intergrain exchange constant to 20% of its bulk value increases $(BH)_{max}$ from about 200 kA/m to 310 kA/m, assuming a grain size of 8 nm. Previously, Fischer and Kronmüller [7,8] studied the influence of intergrain exchange interactions in single-phase and two-phase nano-crystalline NdFeB magnets, using micromagnetic finite element simulations. Partial decoupling of the grains increases the coercive field and decreases the remanence in single phase, nanocrystalline magnets. The reduction of the exchange constant in and in an intergranular phase with a thickness of 3 nm to 20% of its bulk value in decreases the coercive field by a factor 1/2 for a mean grain size of 20 nm and a volume fraction of 50% α-Fe.

This work uses dynamic micromagnetic finite element simulations to investigate the effects of intergranular phases on the magnetic properties of α-Fe/$Nd_2Fe_{14}B$ magnets. The exchange constant, A, is reduced gradually towards the grain boundaries in a simple model system consisting of single soft magnetic grain sourrounded by hard magnetic neighbors. Both the width of the intergranular phase and the amount of reduction of A influence the coercive field, in addition to the grain size. The optimum parameters are derived from the numerical results and applied to large scale simulations using a realistic microstructure. The simulation provide considerable insight

into the mechanisms that determine the remanence and the coercive field. Particularly, the results show how intergrain exchange interactions trigger the nucleation and expansion of reversed domains. Section 2 of the paper presents the micromagnetic and numerical background of the simulations. Section 3 presents the numerical results, and section 4 summarize our findings.

2. Micromagnetic and numerical background

Numerical micromagnetics starts from the total magnetic Gibb's free energy, E_t, which is the sum of the exchange energy, the magneto-crystalline anisotropy energy, the magnetostatic energy, and the Zeeman energy [14]:

$$E_t = \int \left[A \sum_{i=1}^{3} \nabla \beta_i^{\,2} + f_k \boldsymbol{J} - \frac{1}{2} \boldsymbol{J} \cdot \boldsymbol{H}_d - \boldsymbol{J} \cdot \boldsymbol{H}_{ext} \right] dV, \tag{1}$$

where $\boldsymbol{J} = (\beta_1,\beta_2,\beta_3)J_s$ denotes the magnetic polarization. A is the exchange constant and f_k is the energy density associated with uniaxial ($Nd_2Fe_{14}B$) or cubic (α-Fe) magnetocrystalline anisotropy. $\boldsymbol{H}_d$ and $\boldsymbol{H}_{ext}$ denote the demagnetizing and the external field, respectively. The minization of E_t provides an equilibrum distribution of the magnetic polarization. In order to proceed towards the next local minimum of E_t, the Gilbert equation [15]

$$\frac{\partial \boldsymbol{J}}{\partial t} = -|\gamma| \boldsymbol{J} \times \boldsymbol{H}_{eff} + \frac{\alpha}{J_s} \boldsymbol{J} \times \frac{\partial \boldsymbol{J}}{\partial t} \tag{2}$$

is integrated in time. The effective field, $\boldsymbol{H}_{eff} = -\delta E_t / \delta \boldsymbol{J}$, is the variational derivative of the magnetic Gibb's free energy. γ is the gyromagnetic ratio of the free electron spin, and α is the dimensionless Gilbert damping constant. Equation (2) gives the physical path of the system towards equilibrium and is believed to give more realistic values of the coercive field than simple energy minization techniques [16]. The effective field $\boldsymbol{H}_{eff}^{(k)}$ at the node k of an irregular finite element mesh may be approximated using the box scheme

$$\boldsymbol{H}_{eff}^{(k)} = -\frac{1}{V_k} \frac{\partial E_t}{\partial \boldsymbol{J}}, \tag{3}$$

where V_k is the volume associated with the node k. The following conditions hold for the box volumes

$$\sum_k V_k = \int dV, \qquad V_k \cap V_l = 0 \text{ for } k \neq l. \tag{4}$$

The magnetic polarization is defined on the nodal point of the finite element mesh and is interpolated linearly within each finite element. In order to speed up the calculation of the demagnetizing field $\boldsymbol{H}_d$, we introduce a magnetic scalar potential, U, which eliminates the long range terms from Equation (1) [17]. A hybrid finite element / boundary integral method [18] is used for computing the magnetostatic boundary value problem for U. This method requires no elements outside the magnetic particle, to consider the boundary conditions for U at infinity. The time integration of Equation (2) is performed using a combined BDF / GMRES method [19]. Tsiantos and co-workers [20] showed that this method performs considerably better than explicit time integration

schemes like the Adams method for highly exchange coupled systems. For numerical convenience the Gilbert damping constant was set to $\alpha = 1$.

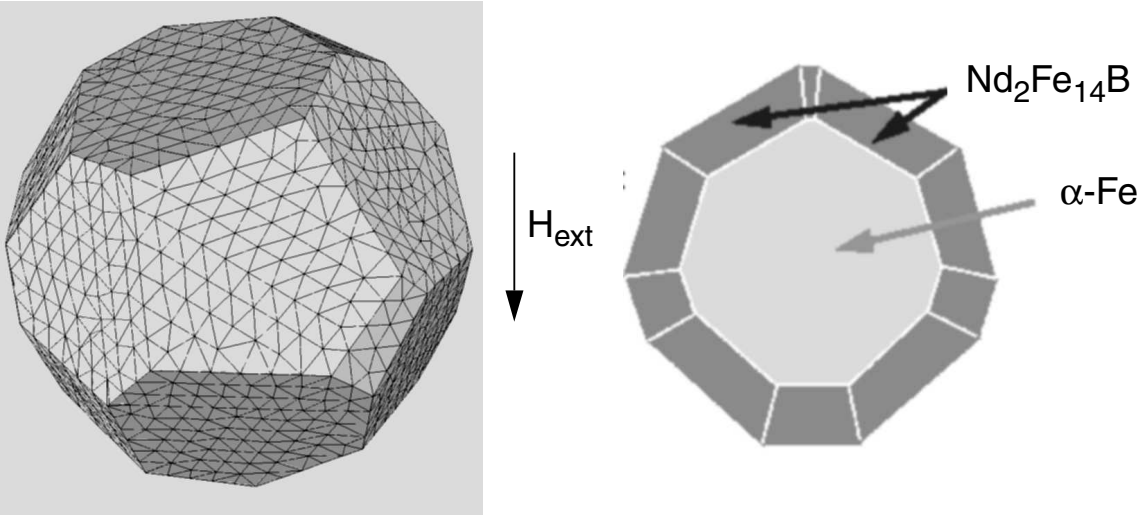

Figure 2: Model system of an exchange-spring magnet consisting of an α-Fe grain and 20 $Nd_2Fe_{14}B$ grains. Left: Finite element mesh at the outer surface of the model. Right: Slice through the model showing the interior α-Fe particle and the sourrounding $Nd_2Fe_{14}B$ grains.

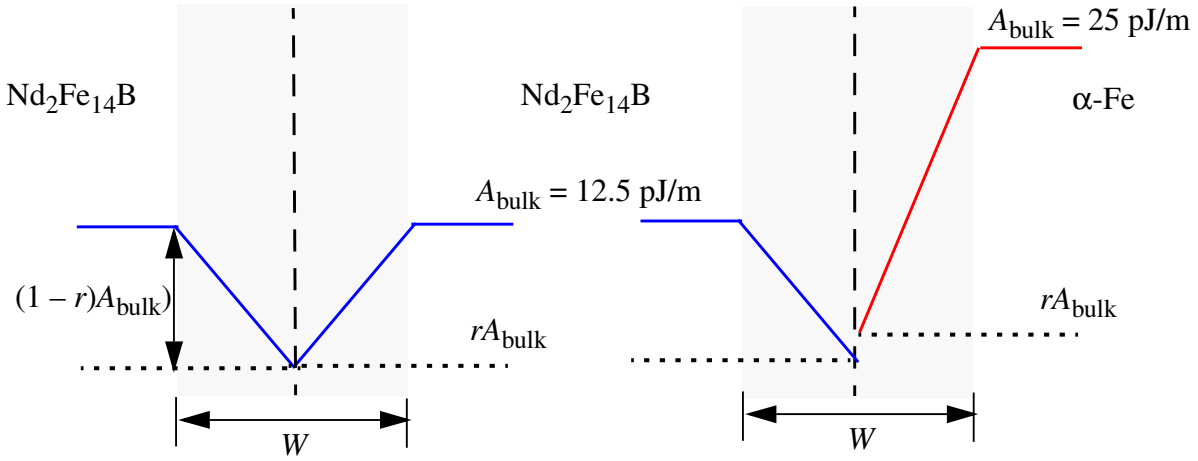

Figure 3: Intrinsic properties of the intergranular phase. Within a region of thickness $W/2$ the exchange constant decrease linearly from its bulk value to rA_{bulk}.

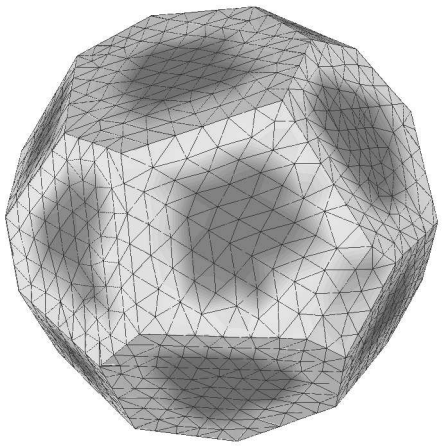

Figure 4: Variation of the the exchange constant near the grain boundaries. The grey scale maps the strength of the exchange interactions, which decrease linearly towards the grain boundaries (W = 3.2 nm, r = 0.2)

3. Results and Discussion

Model system
Figure 2 shows a simple model of a two-phase nanocrystalline magnet. A single α-Fe grain is surrounded by 20 $Nd_2Fe_{14}B$ grains. The anisotropy directions of the hard magnetic grains are randomly oriented. The hard magnetic grains are truncated so that the volume fraction of the soft grains is 36%. The grains are subdivided into tetrahedral finite elements. The total number of elements is 34000. The element size is approximately 1 nm. The grains are either in direct contact or are separated by an intergranular phase of width W. Within this intermediate phase the exchange constant varies as shown in Figure 3. The exchange consant decreases linearly from its bulk value, A_{bulk}, to rA_{bulk} at the interface between two neighboring grains. The same procedure is used for both type of grain boundaries, hard/hard and soft/hard interfaces. The grey scale plot of Figure 4 gives the exchange constant at the surface of the structure.

In addition to the width, W, and the reduction, r, the grain diameter of the α-Fe grain, D, was varied in the calculations. Thus the model system is characterized by the three parameters (W, r, D). Table I gives the intrinsic material parameters used for the calculations.

Table I. Intrinsic Magnetic properties. The spontaneous magnetic polarization, J_s, the bulk value of the exchange constant, A_{bulk}, and the anisotropy constants K_1 and K_2.

	anisotropy	J_s (T)	A_{bulk} (pJ/m)	K_1 (MJ/m^3)	K_2 (MJ/m^3)	
$Nd_2Fe_{14}B$	uniaxial	1.61	12.5	4.6	0.66	[21]
α-Fe	cubic	2.15	25	0.046	0.015	[1]

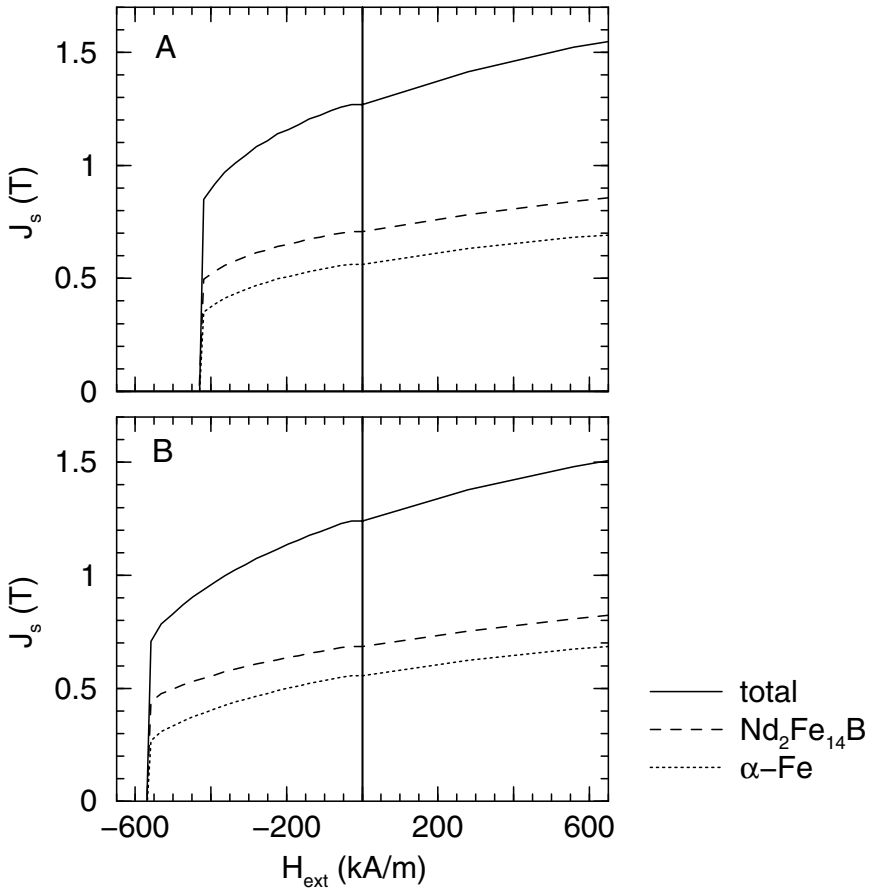

Figure 5: Numerically calculated demagnetization curve for the model system of fig. 1. The grain diameter of the α-Fe grain was 10 nm. A: No intergranular phase, perfect exchange interactions between the grains. B: Intergranular phase with width $W = 2$ nm and reduction $r = 0.2$.

Intergrain exchange interactions and magnetization reversal

Figure 5 compares the numerically calculated demagnetization curves for a system with perfect exchange interactions between the grains A: ($W = 0$, $r = 1$, $D = 10$ nm), and for a system with an intergranular phase B: ($W = 2$ nm, $r = 0.2$, $D = 10$ nm). In addition to the total magnetic polarization, given by the solid line, the graphs give the contributions from the hard magnetic phase (dashed line) and the soft magnetic phase (dotted line). Whereas the intergranular phase has only a minor effect on the remanence, which changes from $J_r = 1.27$ T to $J_r = 1.24$ T, the coercive field increases from $H_c = 440$ kA/m to $H_c = 580$ kA/m, as the intergrain exchange interactions are reduced. Futhermore the overall shape of the demagnetization curve remains the same for both simulations.

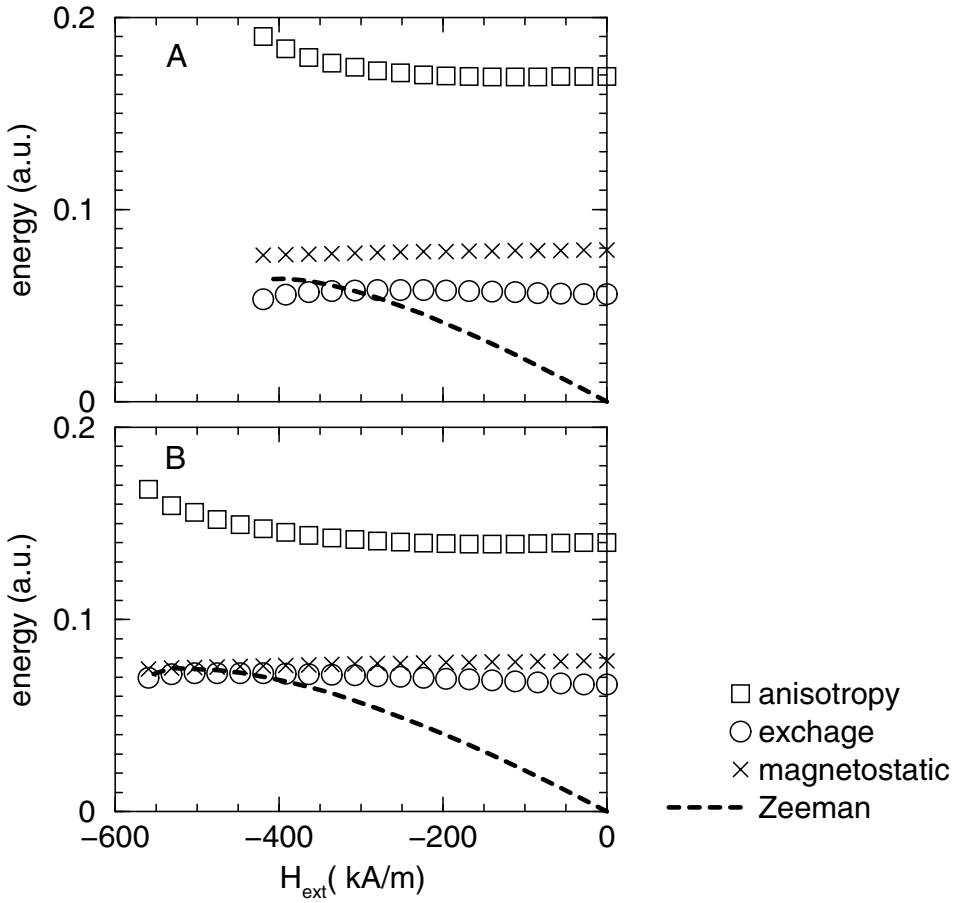

Figure 6: Micromagnetic energy contributions along the reversible part of the demagnetization curve. A: No intergranular phase, perfect exchange interactions between the grains. B: Intergranular phase with width $W = 2$ nm and reduction $r = 0.2$.

The curves denoting the contribution of $Nd_2Fe_{14}B$ and the contribution of α-Fe to the total magnetic polarization are nearly parallel, which indicate that hard and soft phases switch together, when the external field reaches a critical value. For small opposing fields the magnetization of the soft grain rotates reversibly out of its equilibrium direction at zero applied field. During this process the magnetization remains moderately uniform with the α-Fe particle. However, intergrain exchange interactions provide a torque onto the neighboring hard magnetic grains, causing the magnetization to rotate out of their local magneto-crystalline anisotropy axes near the grain boundaries. Since both phases are exchange coupled, the deviations of the magnetization from the local anisotropy axes near the grain boundaries increase with increasing rotation of the magnetization within the α-Fe grain. This gives rise to an increase of the magneto-crystalline anisotropy energy with decreasing external field. This process is more pronounced in system A where the grains are in direct contact. Owing to the perfect coupling the anistropy energy is considerably larger in system A than in system B with reduced intergrain exchange interactions. Owing to the intergranular phase, the magnetization within the α-Fe grain may rotate without causing major deviations of the hard phase magnetization from the local easy axes. This process which finally initiates irreversible switching occurs at much higher opposing fields as compared to perfect coupling. Figure 6 illustrates the change of the micromagnetic energy contributions along the reversible part of the demagnetization curve. Again the shape of the curves are similar for both systems.

However, for perfect coupling reversible rotations take place at the expense of anisotropy energy. Irreversible switching is initiated at the interface between the different phases, when the expense of anisotropy energy becomes too large.

Figure 7 compares the magnetization distribution in the undercritical state, just before irreversible switching is initiated, for the systems A, B, and C:($W = 3.2$ nm, $r = 0.2$, $D = 10$ nm). With increasing width of the intergranular phase the effective coupling between the grains decreases. The plots clearly show that the maximum possible rotation increases with decreasing intergrain exchange interactions. If the external field exceeds a critical value, the rotation of the magnetization withing the soft grain becomes too large and the neighboring hard magnetic grain starts to reverse irreversibly.

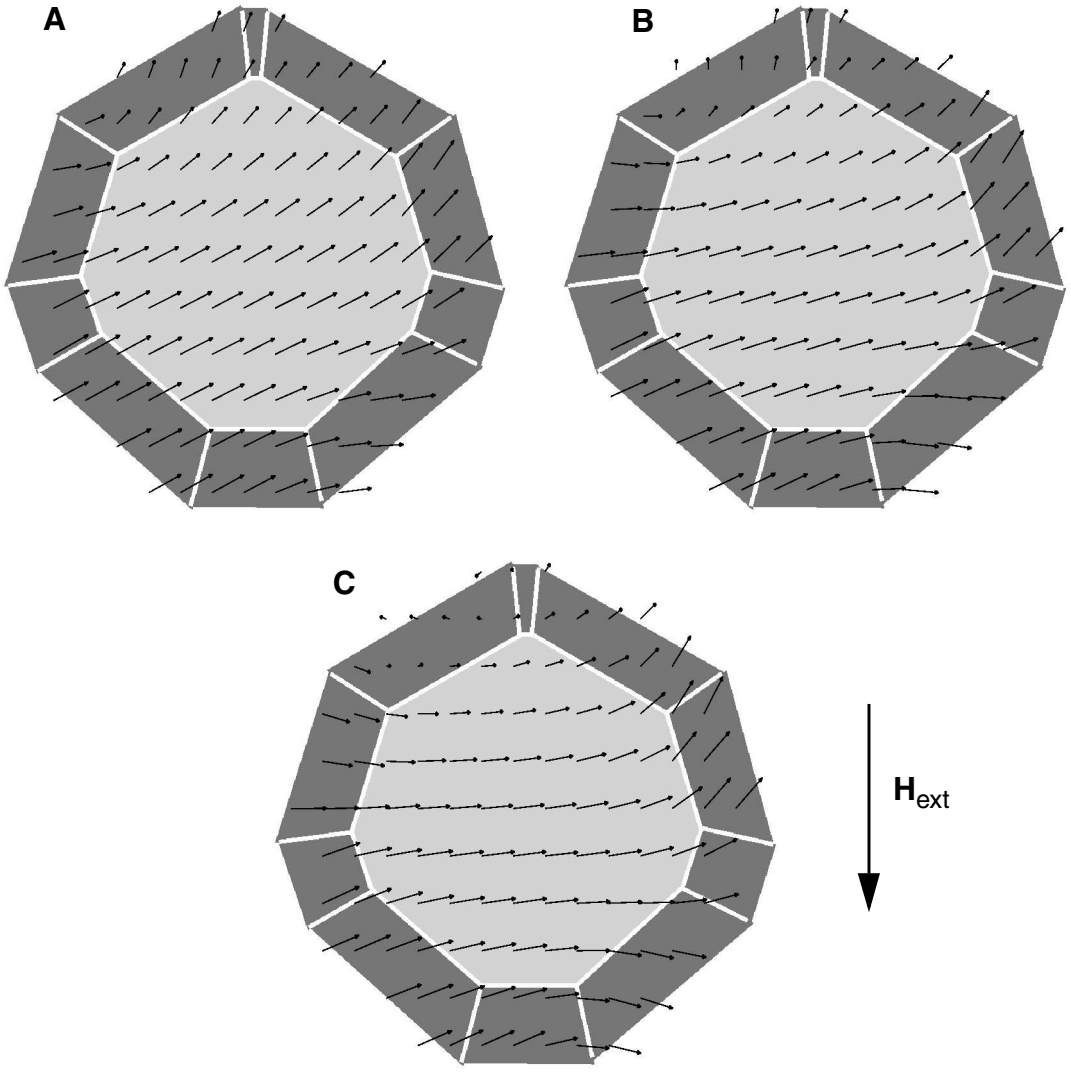

Figure 7: Magnetization distribution in the undercritical state just before irreversible switching is initiated. A: No intergranular phase, perfect exchange interactions between the grains. C: Intergranular phase with width $W = 3.2$ nm and reduction $r = 0.2$. The arrows give the projection of the magnetization onto a slice plane parallel to the external field.

Figure 8 clearly shows that irreversible switching is initated at the interface between the different phases. The plots illustrate the nucleation and expansion of a reversed domain at H_{ext} = 440 kA/m for system A. The reversed nucleus is plotted at different times during irreversible switching. A similar process, which will occur at higher opposing fields, is observed for systems B and C.

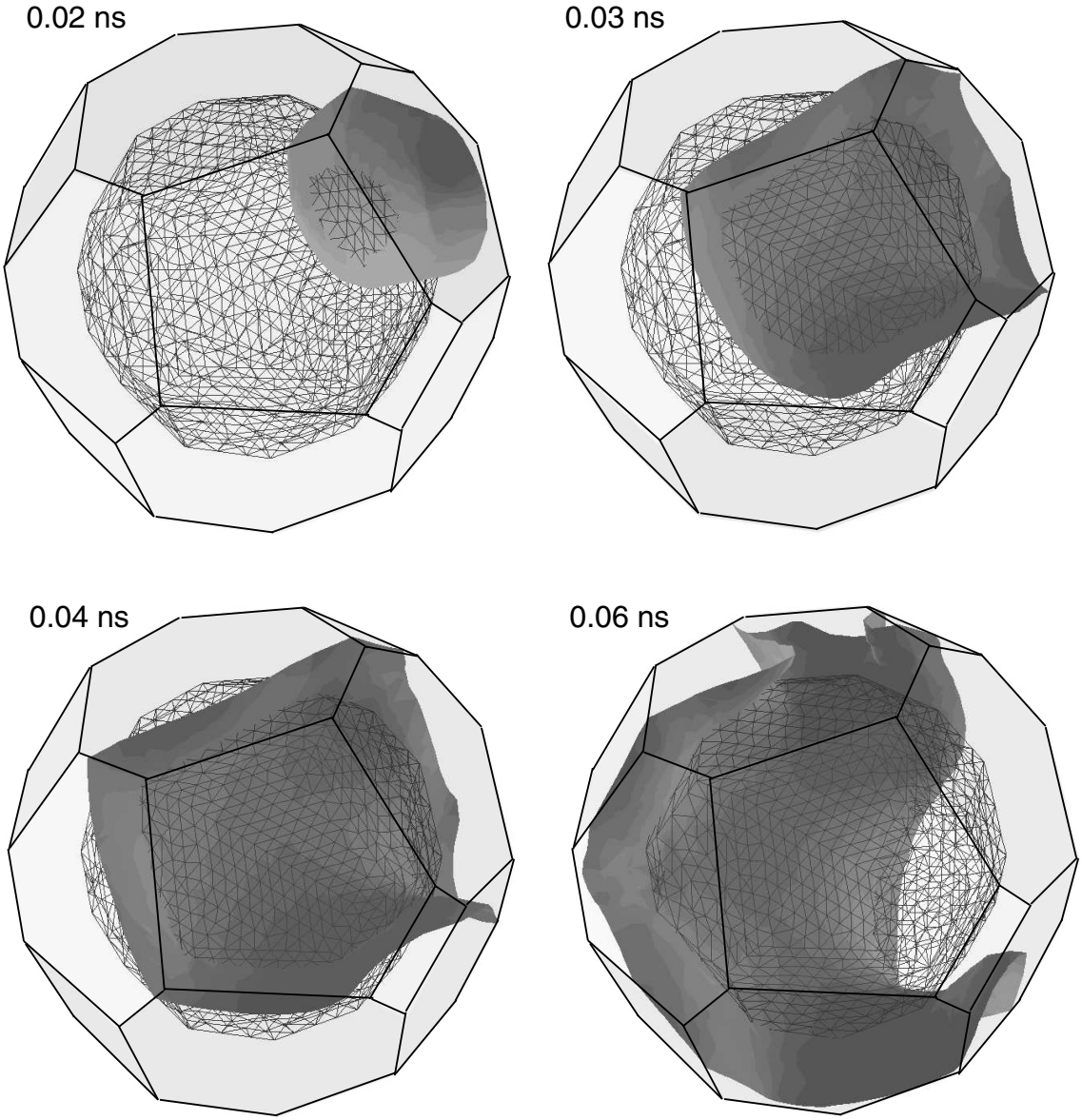

Figure 8: Nucleation of reversed domains in the α-Fe/$Nd_2Fe_{14}B$ model system with perfect exchange coupling. The isosurface indicates the region where the magnetization deviates from the magnetization distribution in the remanent state. In addition the figures show the finite element mesh on the surface of the interior α-Fe particle.

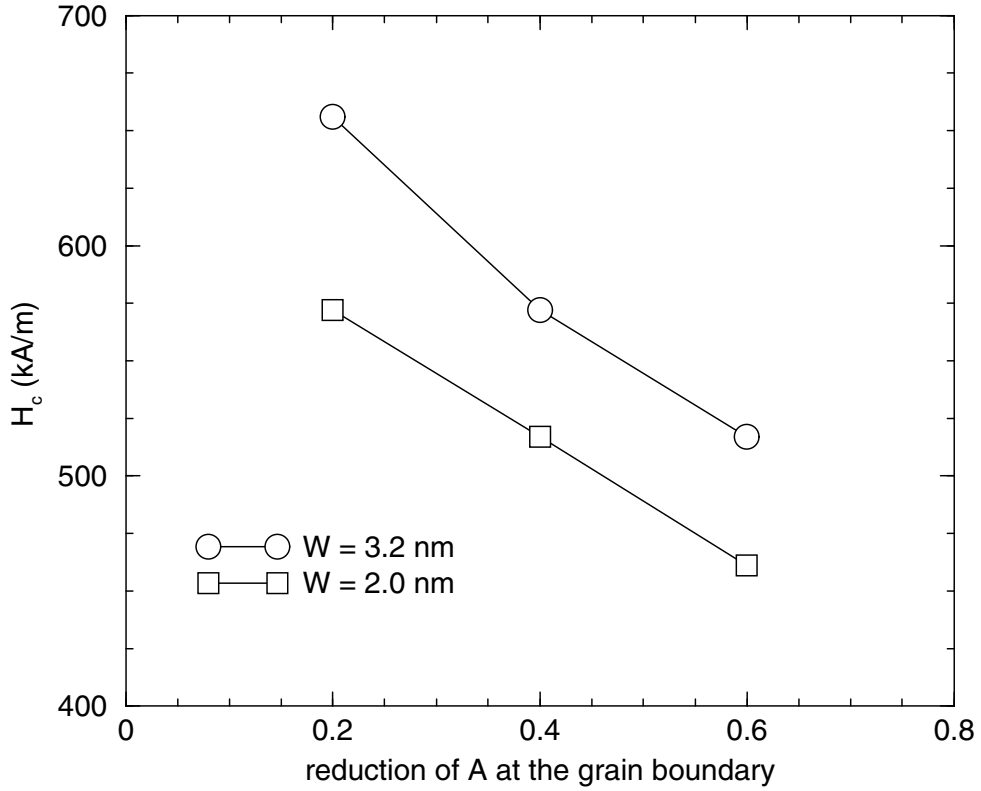

Figure 9: Dependence of the coercive field on the width W of the intergranular phase with reduced exchange interactions. The plots give the coercive field as a function of the reduction r for a grain diameter D = 10 nm.

The numerical results are summarized in Figure 9, which gives the coercive field as a function of of the exchange constant rA_{bulk} next to the grain boundaries. The coercive field increases linearly with r for a grain diameter of the α-Fe grain of D = 10 nm. Increasing the width of the intergranular phase from W = 2 nm to W = 3.2 nm shifts the line towards higher values of the coercive field. Finally, Figure 10 gives the calculated demagnetization curves for different diameters of the α-Fe grain. While keeping W = 3.2 and r = 0.2 constant, D was changed from 10 nm to 20 nm. The results clearly show a grain diameter $D > 15$ nm deteriorates the squareness of the demagnetization curve. The results confirm that an improvement of the magnetic properties due to a remaining amorphous phase is only possible for sufficiently small grain size.

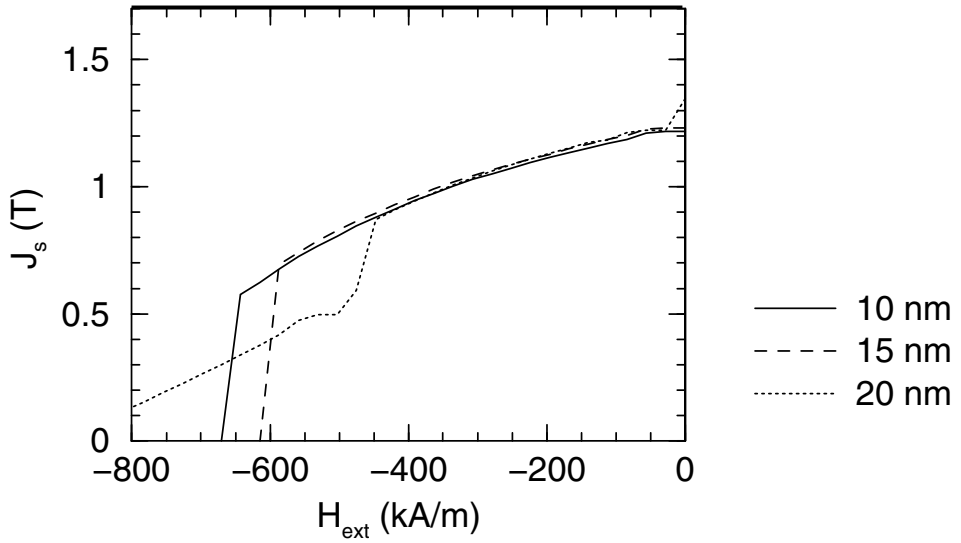

Figure 10: Calculated demagnetization curves as a function of the grain size. Intergranular phase with width $W = 3.2$ nm and reduction $r = 0.2$.

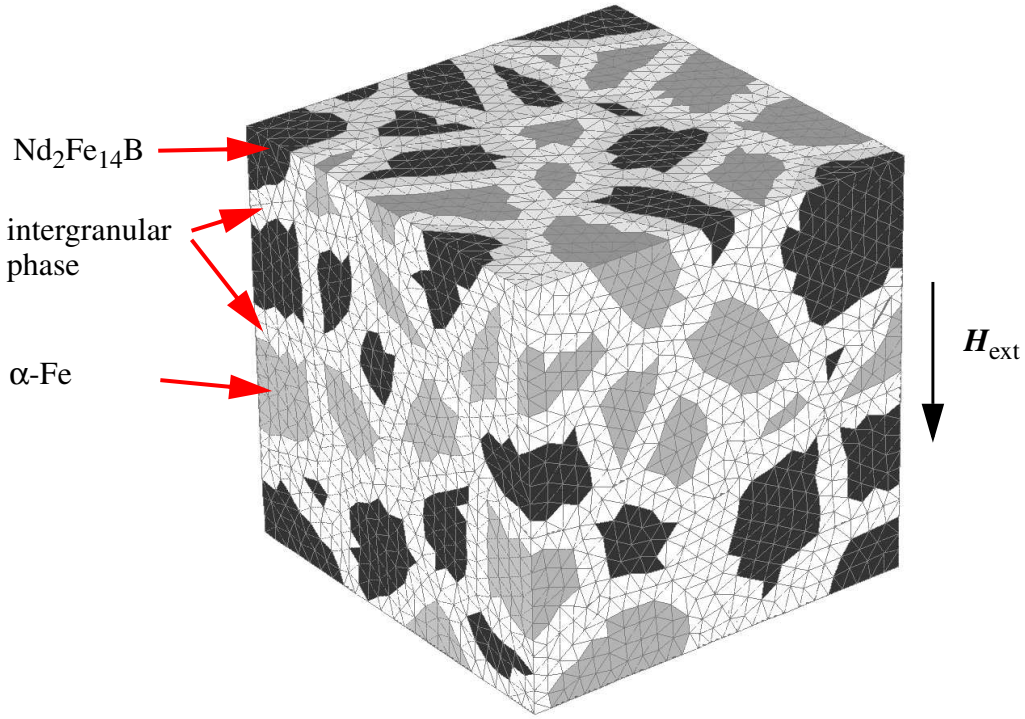

Figure 11: Model of a nanocomposite α-Fe/$Nd_2Fe_{14}B$ magnet with residual amorphous phase, consisting of 125 grains. The volume fraction of α-Fe is 50 %. The mean grain size is 10 nm. The thickness of the amorphous intergranular phase is 3.2 nm.

Complex grain structure

Remanence enhancement and magnetization reversal were simulated for a a realistic grain structure of a two-phase α-Fe/$Nd_2Fe_{14}B$ with remaining amorphous phase, using the optimum parameters W = 3.2 nm, r = 0.2, and D = 10 nm. The grains are obtained from a Voronoi construction [22,23], where the grains are assumed to grow with constant velocity from randomly located seed points. In order to avoid strongly irregular shaped grains the magnet is first divided into cubic cells. Within each cell a seed point is chosen at random. After grain growth simulation, the intrinsic magnetic properties are assigned to the grains such that the volume fraction of α-Fe is 50% and the magneto-crystalline anisotropy axes of $Nd_2Fe_{14}B$ are randomly oriented. Between the grains an intergranular region with reduced exchange constant is assumed in order to mimic the remaining amorphous phase [4]. Figure 11 shows the phase distribution and the intergranular phase at the surface of model magnet, consisting of 125 grains. The mean grain size was 10 nm. The average thickness of the intergranular with was 3.2 nm. The exchange constant of the intergranular phase was reduced to 20% of its bulk value. Now a step function was used to model the decrease of the exchange constant, in contrast to the previous calculations where the exchange constant was reduced linearly towards the interface. This assumption keeps the number of finite elements small as compared to the number of elements required for a gradual change of the intrinsic magnetic properties. The total number of finite elements used to descretize the model show in Figure 11 is about 76000.

Figure 12 shows the magnetization distribution in the remanent state and at applied fields of H_{ext} = – 420 kA/m. The nearly uniform magnetic state for zero applied field gives rise to high remanence. The remanence is J_r = 1.37 T, giving a ratio of the remanent to saturation polarisation is J_r/J_{sat} = 0.73 which considerably exceeds the theoretical limit for the remanence of noninteracting grains. The remanence ratio depends on the crystal symmetry, the crystallographic orientation of the easy directions, and the volume fraction and the saturation polarization of the phases [24]. The remanence ratio a two-phase nanocomposite magnet is

$$J_r/J_{sat} = (1/J_{sat})\{v_1 m_1 J_{s1} + (1 - v_1) m_2 J_{s2}\}, \quad (5)$$

where m_1, m_2 denote the remanence ratio of phase 1 and phase 2, and v_1, v_2 are the volume fraction of the phases. Without any interactions, the remanence ratio of $Nd_2Fe_{14}B$ (uniaxial) and α-Fe (easy-plane) is m_1 = 0.5 and m_2 = 0.83 [25], respectively. For a volume fraction of 50% α-Fe, J_{sat} is J_{s1} + J_{s2}. With J_{s1} = 1.61 of $Nd_2Fe_{14}B$, J_{s2} = 2.15, the remanence ratio of noninteracting particle becomes J_r/J_{sat} = 0.68. The calculated remanence ratio J_r/J_{sat} = 0.73 exceeds this theoretical limit. This result clearly indicates that intergrain exchange interactions enhance the remanence of nanocomposite magnets, even so intergrain exchange interactions are considerably reduce due to the presence of the amorphous phase. The magnetic polarization J is nearly parallel to the anisotropy direction within the hard magnetic grains. Intergrain exchange interactions determine the direction of J within the α-Fe grains, where J is parallel to the average magnetization direction of all neighboring $Nd_2Fe_{14}B$ grains. This average direction corresponds to the saturation direction for an isotropic distribution of the hard phase easy axes. At an external field of H_{ext} = – 420 kA/m the magnetization distribution becomes strongly nonuniform, as the soft magnetic grains revers reversibly. Owing to the reduction of the exchange constant at the interface between the different phases, soft grains may revers while most of the hard magnetic grains remain unswitched. The total magnetic polarization at this field is J = 0.48 T. This value is lower than the correspondig value of the simple model system. Neighboring soft magnetic grains form continuous regions of soft magnetic phase which increases the effective soft magnetic feature size and deteriorates the loop shape.

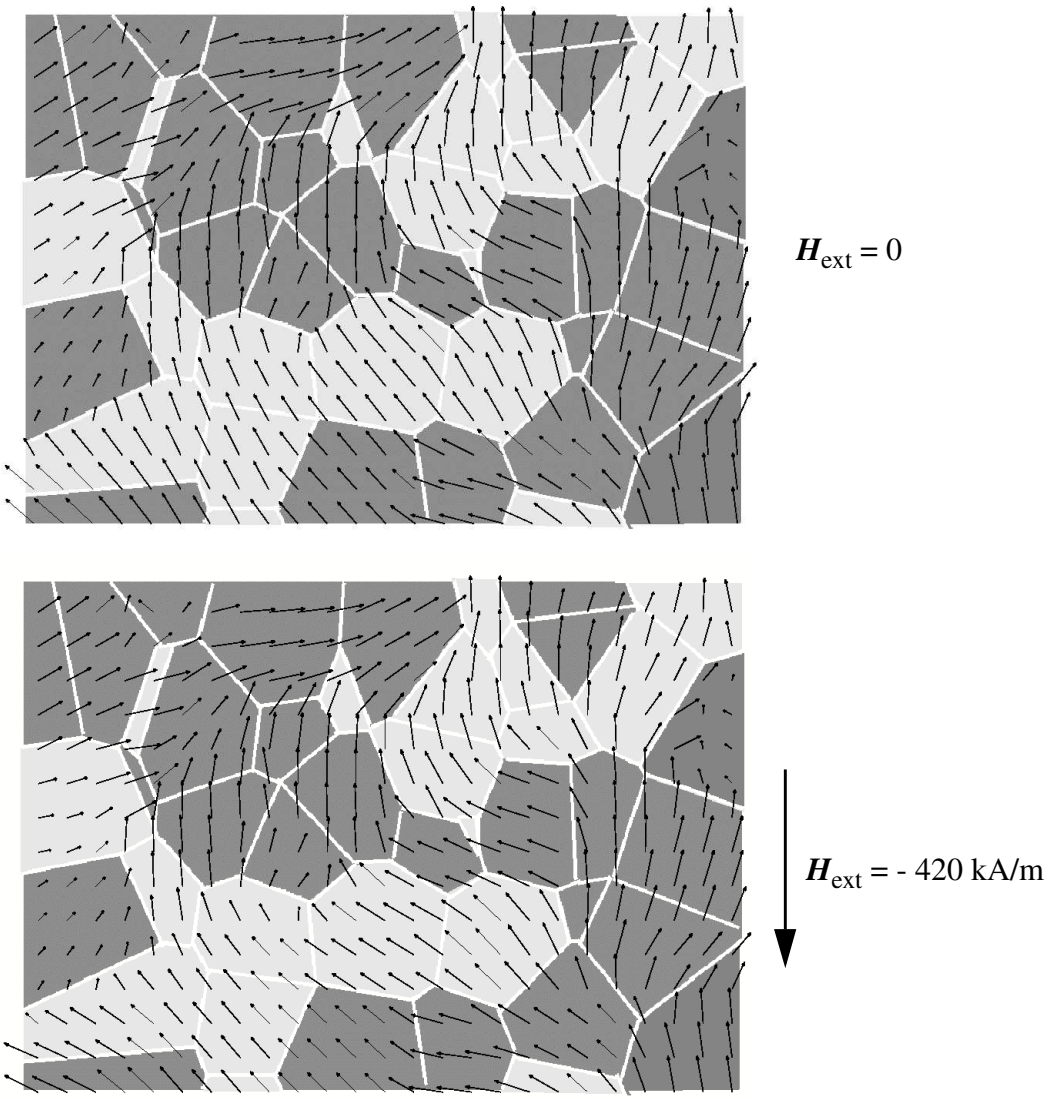

Figure 12: Magnetization distrubution at the remanent state and under the influence of a reversed fields. The arrows give the projection of the magnetization onto a slice plane parallel to the external field. α-Fe may reverse without the switching of neighboring $Nd_2Fe_{14}B$ grains.

4. Summary

Micromagnetic finite element simulation show that an intergranular phase with reduced exchange interactions improves the coercive field of nanocrystalline α-Fe/$Nd_2Fe_{14}B$ magnets, provided that the grain size is sufficently small. The coercive field inreaces from $H_c = 440$ kA/m to $H_c = 660$ kA/m for a mean grain size of 10 nm, without a significant reduction of the remanence, if the grains a separated by an intergranular phase with a thickness of 3.2 nm. The minimum value of the exchange constant in the boundary phase was 20% of its bulk value.

Acknowledgements

This work was supported by the Austrian Science Fund (Y-132 PHY). The authors thank V. Tsiantos for helpful discussions.

References

[1] E. F. Kneller, *IEEE Transactions on Magnetics* **27** (1991) 3588.

[2] A. Inoue, A. Takeuchi, A. Makino, T. Masumoto, *Mater. Trans. JIM* **36** (1995) 962.

[3] M. Hamano, M. Yamasaki, H. Mizuguchi, H. Yamamoto, and A. Inoue, in *Proc. 15th Int. Workshop on Rare-Earth Magnets and their Applications*, ed. L. Schultz and K.-H. Müller (Werkstoff-Informationsgesellschaft, Germany, 1998) p. 199.

[4] Y. Q. Wu, D. H. Ping, K. Hono, A. Inoue, *IEEE Trans. Magn.* **35** (1999) 3295.

[5] T. Kobayashi, M. Yamasaki, M. Hamano, *J. Appl. Phys.* (2000) in press.

[6] H. Fukunaga, J. Kuma, Y. Kanai, *IEEE Trans. Magn.* **35** (1999) 3235.

[7] R. Fischer, H. Kronmüller, *J. Magn. Magn. Mater.* **184** (1998) 166.

[8] R. Fischer, H. Kronmüller, *J. Appl. Phys.* **83** (1998) 3271.

[9] H. Kanekiyo and S. Hirosawa, *J. Appl. Phys.* **83** (1998) 6265.

[10] V. Archambault, D. Pere, *Mat. Res. Proc.* **577** (1999) 153.

[11] H. Hamano, M. Yamasaki, H. Mizuguchi, T. Kobayashi, H. Yamamoto, A. Inoue, *Mat. Res. Proc.* **577** (1999) 153.

[12] V. Panchanathan, *IEEE Trans. Magn.* **31**, (1995) 3605.

[13] J. J. Croat, *J. Appl. Phys.* **81**, (1997) 4804.

[14] W. F. Brown Jr., *Micromagnetics* (Wiley, New York, 1963).

[15] T. L. Gilbert, *Phys. Rev.* **100** (1955) 1243.

[16] R. H . Victora, C. F. Brucker, and F. E. Spada, *J. Magn. Magn. Mater.* **97** (1991) 343.

[17] P. Asselin and A. A. Thiele, *IEEE Trans. Magn.* **22** (1986) 1876.

[18] D. R. Fredkin, T. R. Koehler, *IEEE Trans. Magn.* **26** (1990) 415.

[19] A. C. Hindmarsh, L. R. Petzold, *Computers in Physics* **9** (1995) 148.

[20] V. D. Tsiantos, J. J. Miles, and B. K. Middleton, in *Proc. 3rd European on Numerical Mathematics and Advanced Applications*, *Enumath 99* (World Scientific) .

[21] M. Sagawa, S. Fujimura, H. Yamamoto, Y. Mastuura, and S. Hirosawa, *J. Appl. Phys.* **57** (1985) 4094.

[22] F. P. Preparata, M. I. Shamos, *Computational Geometry* (Springer, New York, 1988).

[23] T. Schrefl, J. Fidler, *J. Magn. Magn. Mater.* **111** (1992) 10.

[24] 1.K. H. Müller, D. Eckert, A. Handstein, M. Wolf, S. Wirth, and L. M. Martinez, in *Proc. 8th Int. Symposium on Magnetic Anisotropy and Coercivity in RE-TM Alloys*, ed. C. A. F. Manwaring, D. G. R. Jones, A. J. Williams, I. R. Harris (University of Birmingham, Birmingham, 1994) p. 179.

[25] G. Bertotti, *Hysteresis in Magnetism -- For Physicists, Materials Scientists and Engineers* (Academic Press, 1998).